

Evaluation of Deployable Aerosurface Systems for Mars Entry



AE8900 MS Special Problems Report
Space Systems Design Lab (SSDL)
Guggenheim School of Aerospace Engineering
Georgia Institute of Technology
Atlanta, GA

Author:
Juan G. Cruz-Ayoroa

Advisor:
Dr. Robert D. Braun

December 14, 2012

Evaluation of Deployable Aerosurface Systems for Mars Entry

Juan G. Cruz-Ayoroa, Robert D. Braun
Georgia Institute of Technology, Atlanta, GA 30332

Joseph A. Garcia, John D. Melton
NASA Ames Research Center, Moffett Field, CA 94035

and

Peter A. Gnoffo
NASA Langley Research Center, Hampton, VA 23681

One of the challenges presented by the exploration of Mars is the entry, descent and landing (EDL) of payloads to the surface. Current robotic missions to Mars are reaching the limit of existing Viking-heritage EDL technologies. A number of EDL technology improvements can be made to extend the capabilities beyond the current landed mass limits, including increasing the entry vehicle hypersonic drag and lift capability. Technologies being currently studied include inflatable aerodynamic decelerators, which are designed to increase vehicle drag. Many of these concepts center on axisymmetric designs, which provide high drag but relatively low lift and are most easily integrated to blunt entry vehicles. However, due to packaging density and launch vehicle fairing constraints, it is likely that future missions will require the use of slender bodies. This study investigates three deployable concepts designed to provide better integration into a slender vehicle while augmenting its performance by increasing its hypersonic drag. The deployable aerosurfaces are applied to a 5 meter diameter slender vehicle for a robotic mission at Mars with entry masses ranging from 10 to 60t. A multidisciplinary design optimization framework is used to estimate the landed mass capability of each system. Results show that the deployable concepts can significantly improve payload mass capability by reducing the terminal propulsion propellant required. Initial feasibility studies show that the concepts are hypersonically statically stable and comply with mechanical and thermal material capabilities.

Nomenclature

C_D	=	drag coefficient
CG	=	center of gravity
CG_x	=	longitudinal location of center of gravity
C_L	=	lift coefficient
C_m	=	pitching moment coefficient
$C_{m\alpha}$	=	pitching moment stability derivative
C_p	=	pressure coefficient
D	=	deployable diameter
g_0	=	Earth gravitational acceleration, 9.806 m/s ²
L	=	deployable length
M	=	Mach number
m_{engine}	=	engine mass
m_{tank}	=	tank mass
p	=	tank pressure
q_∞	=	freestream dynamic pressure
T	=	thrust force
V	=	tank volume
α	=	angle of attack
β	=	ballistic coefficient, ratio of entry mass to drag area
ϕ	=	tank-mass factor
φ	=	parawing inflation angle
ϑ	=	parawing sweep angle

I. Introduction

ON August 5, 2012, the United States successfully landed its seventh robotic mission on Mars. The Mars Science Laboratory mission, with its 900 kg rover, approaches the limits of current Viking-heritage EDL technologies in terms of landed mass and landing site elevation. As outlined by Braun and Manning [1], a number of EDL technology improvements can be made to extend the capabilities beyond the current landed mass limits. These improvements include decreasing entry vehicle hypersonic ballistic coefficient, increasing lift capability, and developing new supersonic decelerators. Technologies currently being studied include inflatable aerodynamic decelerators, which are designed to reduce the supersonic or hypersonic ballistic coefficient of the vehicle through an increase in vehicle drag area. Many of these concepts center on axisymmetric designs, which provide high drag but relatively low lift and are most easily integrated to blunt entry vehicles. However, due to packaging density and launch vehicle shroud constraints, it is likely that missions with landed masses in the order of 10t will require vehicle shapes to be different from the current blunt body shapes. A slender vehicle shape of the same diameter can provide greater volume for its payload and more efficient packaging within the launch vehicle, in addition to providing greater lift and drag area during entry. This study investigates three deployable concepts designed to provide better integration into a slender vehicle. The aim of the deployable aerosurfaces is to augment the slender vehicle performance by increasing its drag while maintaining its favorable lift to drag ratio, thus improving system payload capability by reducing the terminal propulsion mass requirements.

The baseline architecture consists of a slender vehicle with a propulsive terminal descent initiated at supersonic conditions. Three additional architectures are studied, each having a different deployable aerosurface. The goal of this investigation is to obtain an estimate of the landed mass performance gains achievable by these technologies on a robotic-class mission with a landed masses ranging from 10 to 30t. These performance estimates are achieved through a multidisciplinary design optimization of deployable geometry and trajectory, aimed at finding the maximum landed mass capability of each configuration. Engineering-level models appropriate to a design exploration study are used throughout the investigation. A preliminary study on aerodynamic heating and static stability of the vehicles is also presented to shed light on the feasibility of these concepts.

II. Reference Architecture

Every concept was evaluated using the common reference architecture presented in Figure 1. The aerosurfaces are stowed for launch and deployed in space, before atmospheric entry. The entry velocity is 6.75 km/s, consistent with a direct entry. The deployable is used throughout the hypersonic and supersonic phases, where an optimized bank-modulation is employed. At a certain point in the trajectory the deployable and slender vehicle structure is jettisoned, and a propulsive descent is initiated for a soft landing. The jettison procedure could be carried out by one of the methods outlined by the NASA EDL-SA study [3]. One particular possibility would be to split the aeroshell in half, and allow the deployable device to pull the upper section away from the vehicle, thus minimizing the need for vehicle reorientation. The propulsive initiation point is selected such that soft landing conditions are achieved while following a gravity turn using a fixed thrust-to-weight ratio at Mars of three. This thrust-to-weight ratio was selected based on an optimization study performed for a human-class vehicle [4]. This method for calculation of propulsive descent initiation allows for either subsonic or supersonic initiation conditions, thus it is assumed that supersonic retropropulsion is available.

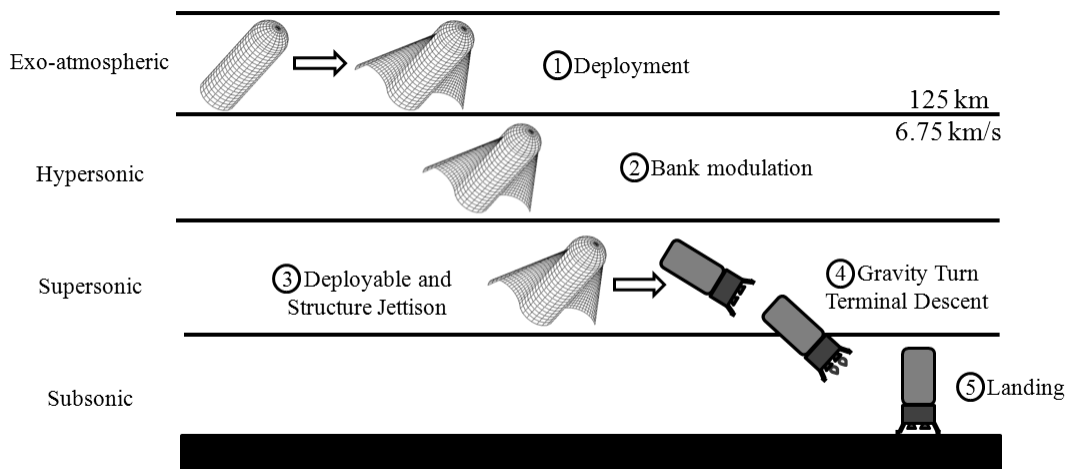


Figure 1. Reference Architecture.

A. Baseline Slender Vehicle

The slender vehicle was represented as a cylinder with a spherical nose cap, and has a length to diameter ratio of 3. This shape has been utilized in multiple conceptual studies of slender entry vehicles [3,5]. A vehicle diameter of 5 meters was selected based on present launch vehicle capabilities, producing a vehicle which is 15 meters long. Based on the payload capabilities of current and planned launchers, it is assumed that a vehicle of this size having a maximum mass of 60t can be delivered to Mars. The selected size and mass range correspond to a maximum packaging density of 262 kg/m³, 25% less than the Apollo capsule packaging density.

B. Deployable Concepts

The three deployable concepts studied are presented in Figure 2. The first concept, known as a parawing, consists of a flexible canopy extended between a rigid leading edge and the slender body, forming a lightweight deployable wing. The leading edges are hinged at the attachment point to the body, allowing them to be folded parallel to the sides of the vehicle for launch and deployed before entry. Multiple NASA wind-tunnel studies have explored the parawing's aerodynamic behavior in subsonic, transonic and supersonic conditions [6,7,8]. Parawings have also been investigated for use as deployable wings for hypersonic entry on Earth [9], and are more recently being studied for use in human-class missions at Mars with landed masses in the order of 40 to 80t [2]. Due to the concave shape of the wings, unique aerodynamic effects have been identified to occur at supersonic and hypersonic conditions and high angles of attack. These effects produce an increase in aerodynamic loads which are detrimental to the static stability of the wing, and may increase aerodynamic heating on the canopy [9,10]. These effects are taken into consideration throughout this investigation. Analytical studies have also shown that the canopy can take different shapes at different angles of attack during hypersonic flight, and this can have a significant impact on the aerodynamic properties of the vehicle [15]. In this study the canopy is modeled as a rigid structure having a conical shape. Possible capabilities of this technology include the use of inflatable leading edges and continuous sweep modulation during entry for active lift, drag and bank control. These ideas are not explored in this study.

The second concept, termed inflatable chines, consists of using inflatable structures on the sides of the vehicle to increase drag area. Although these structures produce less of an area increase, they are lighter and potentially less complex than a parawing. The chines were assumed to have a cylindrical shape, and are located such that their centerlines are aligned with the sides of the slender vehicle.

The third concept uses inflatable structures to emulate a delta wing. Flexible TPS extends between two inflatable conical chines attached to the sides of the vehicle, forming a flat surface. The flat bottom is intended to improve hypersonic lift and drag characteristics, at the expense of mass and complexity. The chine and delta vehicle concepts were inspired by inflatable entry vehicle concepts developed by NASA in the 1960s [23,24].

The leading edges of the parawing are assumed to be made of C/SiC, a high-performance ceramic-matrix-composite material which has been shown to perform safely under load at temperatures up to 1600°C [11] and has been flight-proven in entry conditions on the X-38 vehicle. The canopy is assumed to be made of carbon cloth, a flexible heat-resistant fabric being developed for the ADEPT system [12]. This material is designed to re-radiate heat from the front and back surfaces of the cloth, which are exposed to the flow in the parawing configuration. For the inflatable concepts, a structural fabric layer of Kevlar 49 was used, wrapped in a thermal protection layer of Pyrogel 3350 and SiC fabric. This thermal protection composite is being developed for hypersonic inflatable aerodynamic decelerators, and has been shown to withstand a heat flux of 100 W/cm² for 90 seconds [13]. The area of flexible thermal protection systems is currently in development, and more capable materials can be expected in the future.

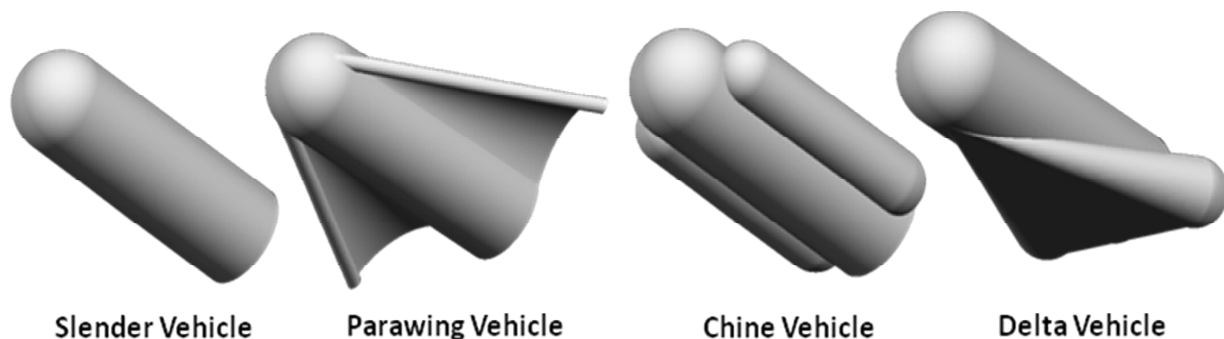


Figure 2. Vehicle configurations.

III. Analysis Methodology

A multidisciplinary design optimization framework was developed as shown in Figure 3. A size-as-you-fly [5] approach was implemented to simplify the subsystem sizing and mass estimation process. Under this approach, the vehicle entry mass and geometry are fixed throughout the analysis, which allows for the propagation of trajectory independently of subsystem mass estimations. Using trajectory results, the mass of the various subsystems can be appropriately sized, and any unallocated mass is designated as payload. This allows the trajectory code to be decoupled of the mass estimation code, and iteration is not required. A Newtonian aerodynamic method is implemented so the aerodynamics of the vehicle is also independent of trajectory flight conditions. The analysis block is wrapped inside a particle swarm optimizer [14] to simultaneously optimize deployable geometry and trajectory parameters using the payload mass fraction as the objective function.

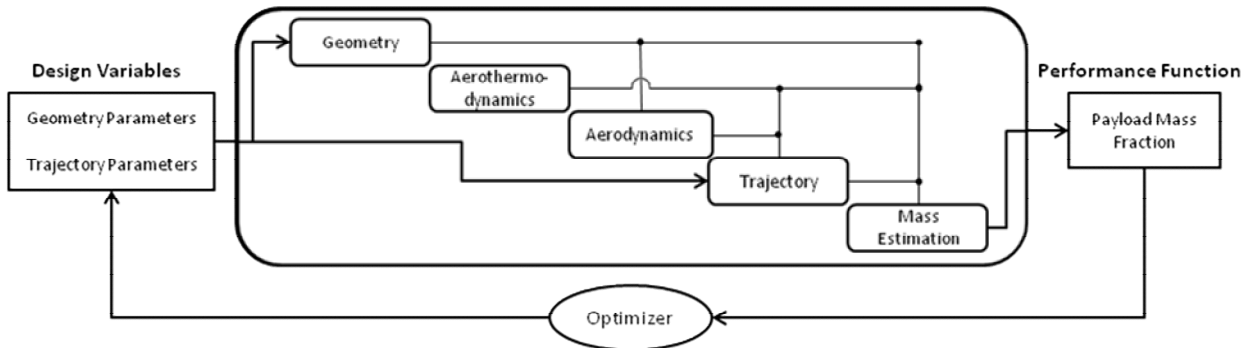


Figure 3. Multidisciplinary design optimization framework.

A. Geometry

The deployable concepts were parameterized as shown in Figure 4. The selected geometric parameters fully define the shape of the deployables and are used as design parameters in the optimization process. The figure illustrates a representative set of meshes created by the parametric mesh generator, which are later used for aerodynamic analysis. The parawing canopy is modeled as a cone with a rigid shape, consistent with previous parawing aerodynamic studies [15]. It should be noted that at least one study has shown that aeroelastic effects on the canopy can have a significant impact on the shape and aerodynamics of a parawing at hypersonic speeds [15]. The leading edge of the parawing has a 0.75 meter diameter. The canopy inflation angle (ϕ) determines the curvature of the canopy; an angle of 180 makes the canopy half of a cone, while an angle of 0 makes the canopy a flat surface.

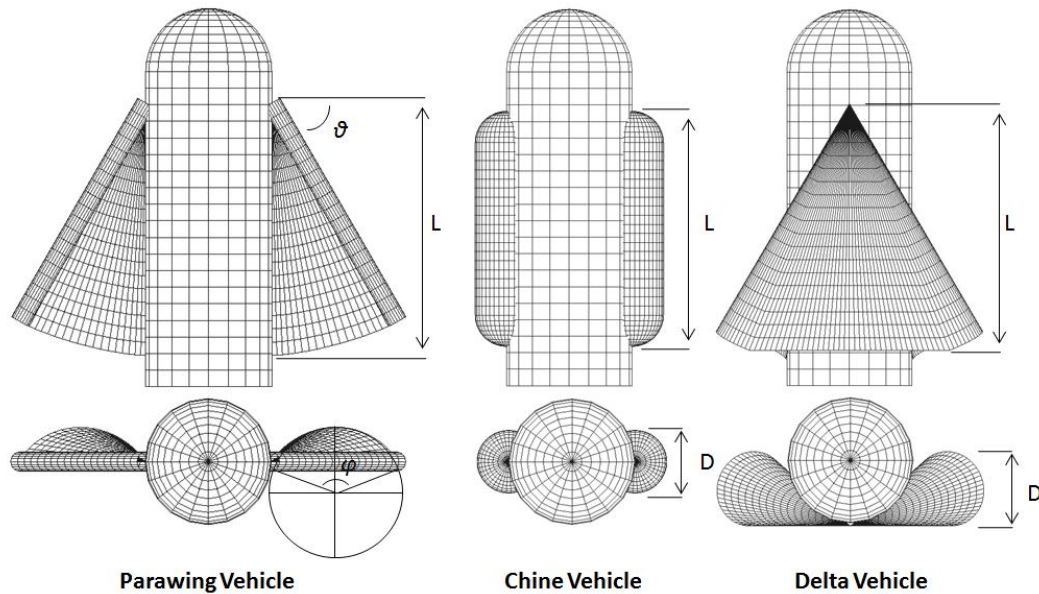


Figure 4. Deployable geometry parameterization.

B. Aerothermodynamics

The CBAERO software package was used to generate aerodynamic heating estimates. CBAERO is an engineering level tool for predicting the aerodynamic and aerothermodynamic characteristics of general vehicle configurations, which has been anchored against high-fidelity aerothermodynamic codes for a geometry similar to the baseline slender vehicle [16]. The standard aeroheating method was used, assuming a Martian atmosphere and a free transition turbulence assumption, unless otherwise stated.

A number of cases were analyzed in CBAERO for the baseline slender vehicle at a nominal angle of attack of 55 degrees, Mach numbers ranging from 1 to 40 and dynamic pressures ranging from 1 kPa to 50 kPa, assuming fully turbulent heating conditions. The averaged heat flux over the slender vehicle forebody was tabulated to form an aerodynamic heating database which is used for TPS sizing calculations. Four additional databases were generated to capture the heat flux experienced by the critical heating points of each concept with the purpose of imposing trajectory heating constraints. For the slender vehicle, the maximum heating seen by the forebody was used. For the chine and delta concepts, the maximum heating seen by the inflatable structures was used for the database. For the parawing concept, although the leading edge is expected to experience high localized heating, it is assumed that the canopy will be the critical heating point. This is because the leading edge is rigid, and it is assumed that capable rigid TPS materials can be used to protect it. Additionally, it is expected that shock interaction effects will create high localized heating on the canopy, which is made of less capable, flexible TPS materials. A parawing arc-jet study carried out on an 8.6 inch model of similar parawing geometry determined that the shock effects could increase the heating in the canopy up to five times [9]. Based on this information, the maximum canopy heating calculated by CBAERO was multiplied by a factor of five to form the parawing database. All of these databases were generated for vehicles assuming a nominal set of geometry parameters and an angle of attack of 55 degrees.

Since significant uncertainty exists on the capabilities of future flexible TPS materials, a nominal heat flux limit of 150 W/cm² was used for all deployable concepts, and an additional case was run using a limit of 100 W/cm² to explore the sensitivity of the results to these constraints. A 500 W/cm² limit was used for the slender vehicle, corresponding to the capabilities of rigid TPS materials.

C. Aerodynamics

The supersonic and hypersonic aerodynamic performance of the vehicles was approximated by applying the Newtonian aerodynamic approach to the meshes created by the parametric mesh generator. The Newtonian aerodynamic approach is not expected to be particularly accurate for the parawing geometry due to the strong influence of shock interactions on pressure distributions on the wing [10]. To examine the importance of these effects on the aerodynamic performance, and the effect this has on the landed mass performance, the optimized geometry for the 60t case was analyzed using the Cart3D CFD software package to generate a database of aerodynamic coefficients as a function of Mach number. This database was then used to run the trajectory optimization again, keeping the geometry constant, to examine the impact on the landed mass. The Cart3D results were also used to analyze the hypersonic and supersonic static stability of the parawing vehicle. The Cart3D CFD software package was selected because it has been validated against experimental data for a similar parawing geometry at supersonic conditions [10].

D. Trajectory

The trajectory of the vehicle was propagated using the 3-DOF equations of motion on a spherical rotating planet [17]. The Mars Gram atmospheric model was used for atmospheric density and temperature estimation. The variables used for the trajectory optimization consist of 10 bank angles spaced evenly over a velocity range of 6.75 km/s to 0 km/s, the initial flight path angle, and the trim angle of attack of the vehicle, which was maintained constant throughout the trajectory. A constant-thrust gravity turn guidance was employed for the propulsive descent in order to capture the upper performance bound on the terminal descent system. The initiation conditions for the gravity turn are selected such that terminal conditions of 0 km altitude and 0 m/s velocity are attained while using a thrust-to-weight ratio at Mars of 3.

A number of constraints were imposed on the trajectory. The maximum acceleration was constrained to 10 Earth g's, consistent with a robotic mission. A maximum skip altitude of 150 km was used. Also, maximum heat flux constraints were imposed based on the requirements of each concept, as explained in section B.

E. Mass Estimation

The entry mass of the system was assumed to be composed of payload mass plus subsystem masses, consisting of vehicle structure, deployable system, reaction control system (RCS), propulsion system, and thermal protection system (TPS). After the mass of each subsystem is calculated based on geometry, aero-thermodynamic, and trajectory results, the payload mass is calculated as the difference between entry mass and total subsystem mass.

i. Vehicle Structure

The slender vehicle structural mass was estimated using a regression developed by the EDL-SA study for the same geometry [18]. This regression is a function of entry mass, vehicle dimensions, maximum entry dynamic pressure, and maximum lateral and axial accelerations. Since the scale of the vehicle being studied falls outside the regression limits, the mass was calculated for a vehicle of 30 meters in length and scaled down to half the size based on vehicle surface area, leading to a multiplication factor of 0.25. A mass margin of 25% is added based on EDL-SA recommendations.

ii. Thermal Protection System

TPS mass was calculated for the forebody of the slender vehicle only. A time-profile of average heat flux over the surface of the vehicle's forebody is first calculated using Mach number and dynamic pressure profiles from the trajectory simulation, and the slender vehicle aero-thermodynamic database developed from CBAERO results. The 1-D heat equation is then solved numerically over this heat flux profile, assuming radiative equilibrium in the surface and an insulated bondline [19]. The required thickness of the TPS is then selected in order to maintain a bondline temperature of 520 °C. This thickness is assumed to approximate the average TPS thickness over the forebody of the vehicle, and is multiplied by forebody surface area and TPS density to obtain total TPS mass. A PICA TPS material was assumed. A 10% mass margin was added to account for attachment mass, and an additional 30% margin was applied to account for uncertainties.

iii. Deployable

Simplified mass models were generated for the three deployable concepts. The mass models are a function of aerodynamic loads and are not dependent on aerothermodynamic loads.

a. Parawing Deployable

The parawing mass model consists of leading edge mass and canopy mass, plus margins. The leading edge was modeled as a hollow cylindrical cantilever beam with distributed aerodynamic and canopy-tension loads. The total normal load generated by the canopy is calculated using Newtonian aerodynamics at maximum dynamic pressure conditions. Previous studies have shown that shock interactions can significantly increase the pressure over the surface of the canopy [10]. Based on this information, the canopy load was increased by 25%. It is expected that the canopy tension will create a triangular distributed load on the leading edge [9]. Assuming that half of the canopy load is taken by the leading edge and half by the body, the magnitude of this distributed load can be calculated. Similarly, the aerodynamic load on the leading edge is calculated by obtaining the total aerodynamic force on the leading edge using Newtonian theory and distributing the load uniformly along the beam. The bending moment at the leading edge resulting from the loads can then be calculated. It is conservatively assumed that both loads act in the same direction and therefore the bending moments can be added together. Knowing the bending moments, the required thickness of the beam at any location can be calculated by solving the cantilever beam stress equations for the beam thickness. Knowing the dimensions of the leading edge, the mass can be calculated by multiplying its volume times the material density. The canopy mass was calculated based on surface area and flexible TPS material areal density. An areal density of 1.96 kg/m³ was used for the carbon cloth material.

A margin of 15% was added to account for the hinge and deployment mechanism, and an additional 50% margin was added to account for additional mass growth.

b. Chine Deployable

The chine mass model is based on structural fabric mass, TPS fabric mass, inflation gas and gas generator mass, plus margins. The structural fabric mass is calculated by sizing the required thickness of Kevlar 49 material to withstand the gauge pressure of the inflatable. This is done by using the thin pressure vessel circumferential stress equation using the chine radius. The internal pressure is taken as 10 times the dynamic pressure. Once the thickness is known, the material volume and mass can be calculated.

Additional mass is added to account for the flexible TPS. The TPS mass is calculated by multiplying the TPS areal mass by the deployable surface area, assuming an areal mass of 1.96 kg/m³ for the Pyrogel 3350 and SiC fabric composite [13].

The mass of the required inflation gas can be calculated using the ideal gas equation. An inflation gas temperature of 423 K was assumed, with a specific gas constant of 297 N-m/kg-K, and the gas generator mass was taken as an additional 1/3 of the inflation gas mass, as done in previous studies [20].

c. Delta Deployable

The delta chine equation mass is estimated using the same procedure as the chine mass estimation, but using the surface area and volume equations appropriate for this geometry. Additional surface area has to be added to account for the fabric forming the flat bottom of the deployable.

iv. Reaction Control System

A reaction control system is sized to provide 30 m/s of velocity change with a 200 second specific impulse using the rocket equation, resulting in 1% of the entry mass. Propellant tank and engine mass are taken to be an additional 0.5% of the entry mass.

v. Propulsion

The propellant mass for the terminal descent propulsion system is sized based on the rocket equation. The required velocity change is calculated from the actual velocity change incurred during the gravity turn plus the gravity losses. Thrust vectoring losses were assumed to be zero due to the gravity turn guidance used. Drag losses were also assumed to be zero, as previous studies have shown that aerodynamic drag can be negligible when high retropropulsion thrust coefficients are used [22]. A liquid bipropellant engine using liquid oxygen and methane at an oxidizer-fuel ratio of 3.5 is assumed, providing a specific impulse of 350 seconds. The mass of the tanks is calculated using the following relation:

$$m_{\text{tank}} = \frac{pV}{g_0 \phi}$$

Where p is the operating pressure of the propellant (taken as 2.8 MPa), V is the propellant volume in cubic meters, g_0 is Earth's gravitational constant, and ϕ is the tank-mass factor, assumed to be 5000 m for titanium [5]. The mass of the engine is approximated using a historical regression [21]:

$$m_{\text{engine}} = (0.00144)T + 49.6$$

Where T is the thrust in Newtons and m_{engine} is the engine mass in kg. A 35% margin is applied to propellant mass, and a factor of 2 and 1.5 is applied to the engine and tank mass, respectively.

vi. System Margin

In addition to the mass margins applied to each subsystem, a system margin of 45% is applied to all systems. This margin is based on EDL-SA methodology [3].

F. Design Space

Table 1 shows the design variables limits imposed in this study. The maximum deployable length is equal to the slender vehicle cylinder length. For the parawing concept, the minimum canopy inflation angle is 100° to avoid an unrealistically flat shape. The maximum chine and delta deployable diameter is equal to the slender vehicle diameter.

Table 1. Design Variable Limits

Design Variable	Minimum	Maximum	Units
Trajectory			
Entry flight path angle	-20	-5	degrees
Bank angle	0	180	degrees
Angle of attack	35	55	degrees
Parawing Vehicle			
Length (L)	2.5	12.5	meters
Sweep (θ)	60	75	degrees
Canopy inflation angle (ϕ)	100	180	degrees
Chine Vehicle			
Length (L)	2.5	12.5	meters
Diameter (D)	0.2	5.0	meters
Delta Vehicle			
Length (L)	2.5	12.5	meters
Diameter (D)	0.2	5.0	meters

IV. Results

A. Aerodynamic Comparison

i. Aerodynamic Performance

Figure 5 provides a comparison of the aerodynamic performance of the optimized vehicles for the 60t entry mass case. Each curve represents a vehicle and each data point an angle of attack. A general trend can be observed that larger angles of attack produce lower ballistic coefficients and lower lift to drag ratio. Since a lower ballistic coefficient is generally more beneficial to landed mass than a higher lift to drag ratio, the optimizer chose the highest allowable angle of attack for all the cases, which is 55 degrees. At this angle of attack all three deployable vehicles have significantly lower ballistic coefficients than the slender vehicle. At the trim angle of attack of 55 degrees, the slender, delta, chine and parawing ballistic coefficients are 1032 kg/m², 677.6 kg/m², 539.1 kg/m² and 487.2 kg/m², respectively. Still, it should be noted that these ballistic coefficients are at least 3 times larger than anything flown to date on Mars.

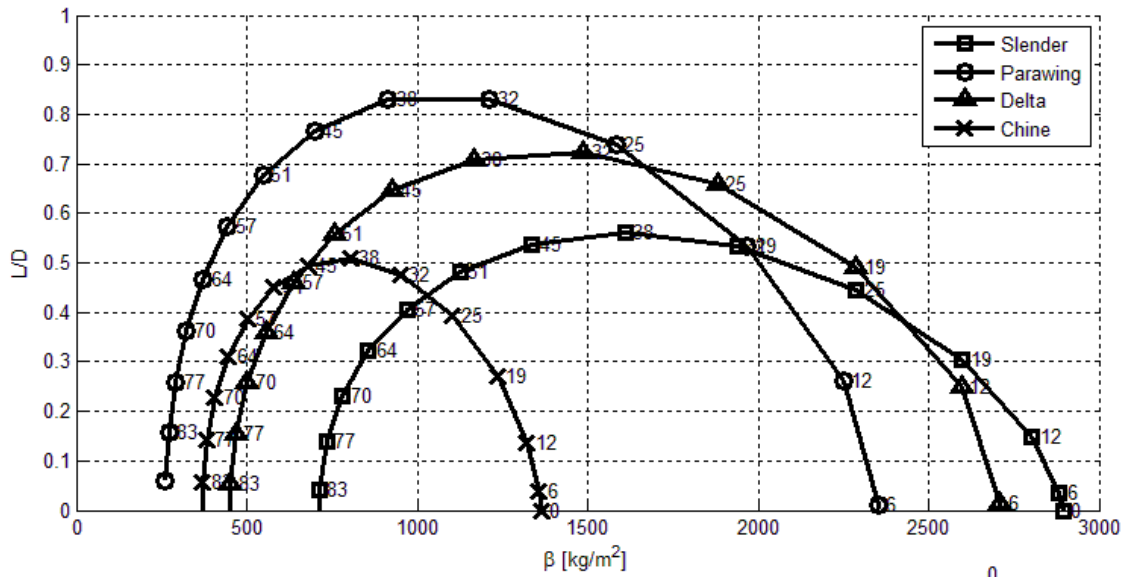


Figure 5. Aerodynamic performance comparison.

ii. Hypersonic Static Stability

As shown in Table 2, all the vehicles are able to trim at the required angle of attack of 55 degrees at hypersonic conditions, and all three deployable concepts increase the hypersonic static stability of the baseline slender vehicle. Additionally, if the center of gravity is assumed to be located along the axis of symmetry of the slender vehicle, the required longitudinal location falls within 5% of the center, except for the parawing concept, which requires the center of gravity to be located farther aft. These results were obtained using the optimized geometries for the 60t entry mass case.

Table 2. Vehicle Hypersonic Static Stability, 60t Entry Mass Case

Vehicle	C_{m_α}	CG_x	Method
Slender	-1.123e-3	0.49	Newtonian
Chine	-2.32e-03	0.51	Newtonian
Delta	-1.188e-3	0.55	Newtonian
Parawing	-6.024e-3	0.62	Cart3D, M = 10

* $\alpha = 55^\circ$, CG along slender vehicle axis of symmetry

iii. Parawing Vehicle Aerodynamics

The Cart3D aerodynamic results shed new light into the aerodynamic properties of a parawing and slender body combination. Figure 6 shows contours of Mach number and surface pressure coefficient for a freestream Mach number of 10 and angles of attack of 55 and 70 degrees. The 55 degree case shows distinct bow shocks generated by the slender vehicle and by the leading edges of the parawing. The bottom surface of the parawing clearly shows an area of high pressure caused by the bow shock of the slender body interacting with the canopy. When the angle of attack is increased to 70 degrees, the bowshocks appear to merge together, and the pressure under the wing becomes more uniform. This effect has been observed in experimental data for a similar parawing geometry at supersonic conditions [10].

Figure 7 shows the aerodynamic coefficients computed by Cart3D. The reference area was taken as the area of the slender vehicle circular cross-section, and the reference length is the total vehicle length. The Mach 10 line shows that the effect of the bowshock merge does not cause a very noticeable effect on the lift and drag on the vehicle. However, the moment coefficient curve has a very sharp slope change at an angle of attack of 65 degrees, which coincides the bowshocks merging. The slope of the curve changes from negative to positive, indicating a destabilizing effect on the vehicle. The Mach 5 and 2.5 lines also show this effect, only at lower angles of attack. These results are consistent with previous experimental and computational data for a similar geometry [10]. Despite this effect, the vehicle is statically stable at 55 degrees angle of attack at Mach 10 and 5. However, it becomes statically unstable at Mach 2.5, implying that this vehicle is not stable at supersonic conditions and a 55 degrees angle of attack. This means that this concept should not be used supersonically, or the vehicle angle of attack has to be decreased at supersonic conditions to maintain stability.

Figure 7 also shows a comparison of the Newtonian aerodynamic results to the Cart3D results. Comparing the Mach 10 results to the Newtonian results, we can observe that the Newtonian method captures the trends and the locations of the maximums well, but differs significantly in the magnitudes. This is because the Newtonian method does not capture any of the shock effects affecting the parawing. From these curves it is easily seen that the net effect of the shock interaction effects is to increase the lift, the drag, and the lift over drag of the vehicle, while reducing the static stability high angles of attack. As such, we should expect the landed mass performance of the parawing vehicle to be better than what would be predicted using a Newtonian aerodynamic analysis. As an example, the 60t entry mass case was re-optimized using Cart3D aerodynamics and the results showed that the parawing aerosurface improved the landed mass of the system by 15.9%, as opposed to the improvement of 13.3% that was obtained using Newtonian assumptions.

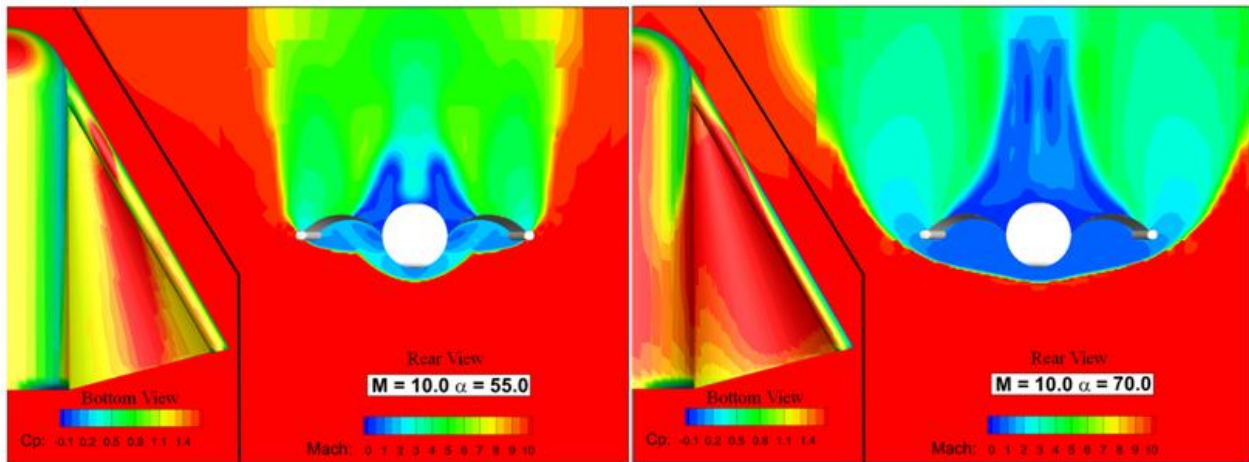


Figure 6. Cart3D Solutions for Parawing Vehicle

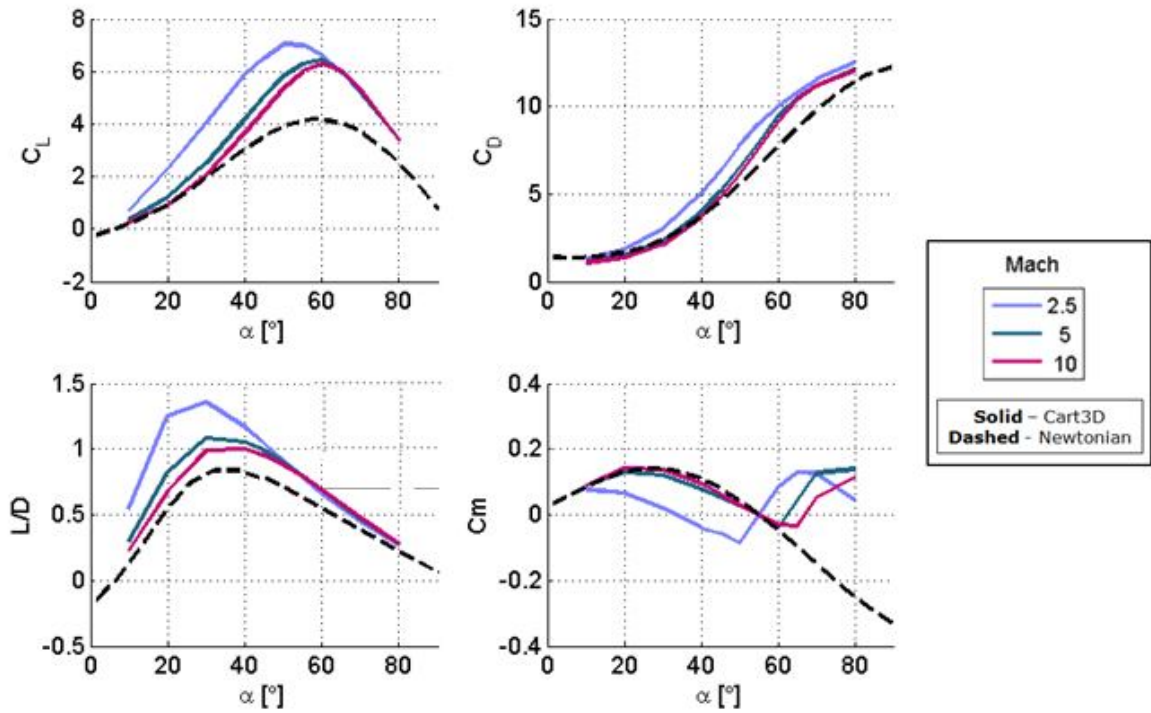


Figure 7. Parawing concept aerodynamic coefficients, 60t entry mass case.

B. Landed Mass Comparison

Figure 8 shows the results of the optimization process for all the architectures. These results show that a slender vehicle of this scale would have relatively poor performance at entry masses below 20t. At this entry mass range the vehicle structure and terminal descent propellant make more than 50% of the entry mass. Blunt bodies are known to be more mass efficient in terms of structural and TPS mass requirements [5], and therefore could potentially perform better in this mass range. However, assuming a 5-meter diameter blunt vehicle with a high-volume shape like the SpaceX Dragon capsule, and using the high Apollo command module packaging density of 350 kg/m³, the maximum entry mass of a 5 meter diameter blunt body would be around 15t. Therefore a slender vehicle may be needed to enable missions with entry masses above 15t, if the diameter is constrained to 5 meters. In the 20 to 60t entry mass range, the slender vehicle performs well, with payload mass fractions of about 0.55. However, the performance starts to decrease at an entry mass of about 40t due to the large retropropulsion propellant mass requirements. Figures 8 and 9 show that the use of a deployable diminishes this effect, enabling higher payload mass fractions.

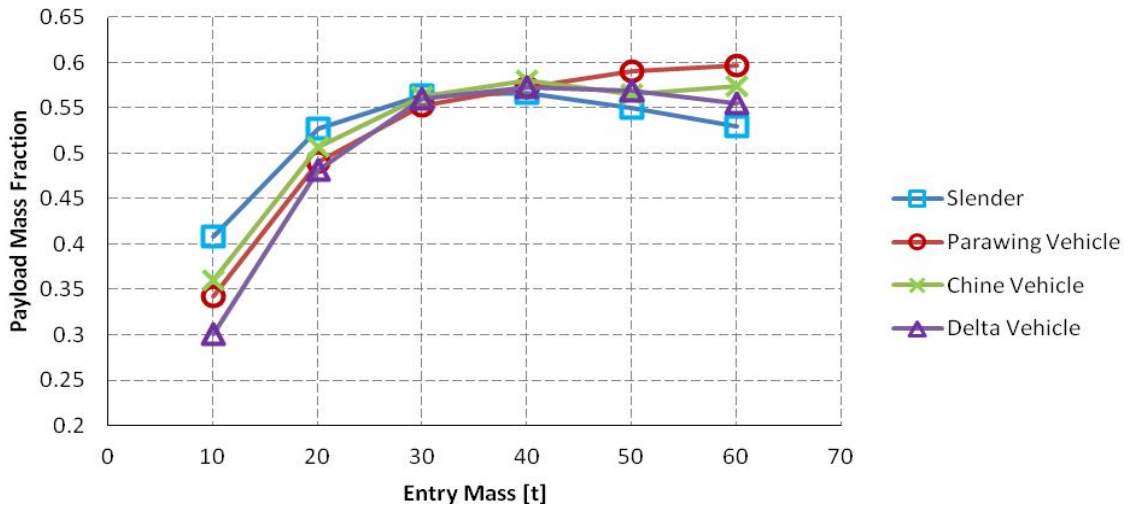


Figure 8. Payload mass fraction vs. entry mass

Figure 9 shows more clearly the effect of the deployables on the landed mass performance relative to the baseline slender vehicle. At low entry masses, the deployable can have a detrimental effect on the landed mass, as the deployable weighs more than the terminal propulsion mass saved. With increasing entry mass, the deployable becomes more beneficial, achieving upwards of 10% landed mass improvement at 60t. The parawing deployable shows significantly better performance improvements relative to the chine and delta deployables. This can be attributed to the larger drag area increase achievable by this technology. As already noted, these results were calculated using a Newtonian aerodynamic model, which provides a conservative estimate of the aerodynamic performance of the parawing. Using high fidelity CFD aerodynamic data, the payload mass improvement of the parawing for the 60t entry mass case jumps from 13.3% to 15.9%.

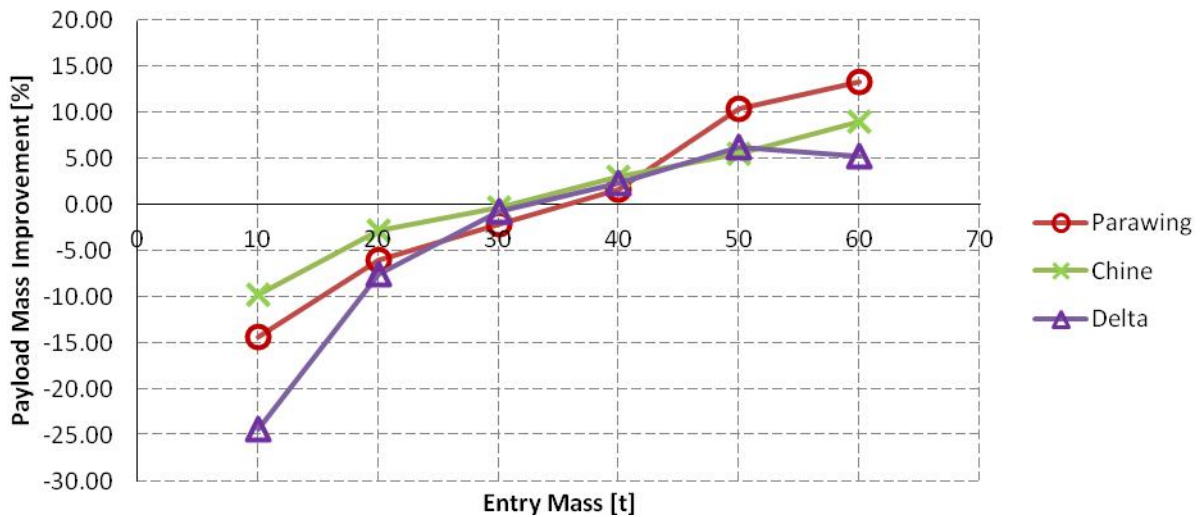


Figure 9. Payload mass improvements achieved by deployable systems.

C. System Mass Comparison

Figure 10 shows a breakdown of the system mass for the 10t, 30t and 60t entry mass cases. The 10t entry mass results show that at this entry mass, the aeroshell structural mass makes about 30% of the system mass, which leads to poor payload mass fraction performance. For the 10t and 30t cases, the optimizer drove down the size of the deployables to a minimum, leading to very small deployable masses and small propellant mass savings. However, looking at the 60t case, it is evident that the main effect of a deployable is a significant the reduction of the terminal descent propellant mass. This is achieved through a reduction in terminal descent delta-V due to the higher drag of the vehicle. The deployables also decrease the required TPS mass by about 13 to 29%, through a reduction in maximum heat flux and total heat load. However, the TPS mass forms a smaller fraction of the entry mass and therefore has a smaller impact on the landed mass. The deployable masses for the 60t entry mass case are significant, and are comparable to the slender vehicle structural mass. The chine concept is the lightest deployable, followed by the delta concept and then the parawing deployable.

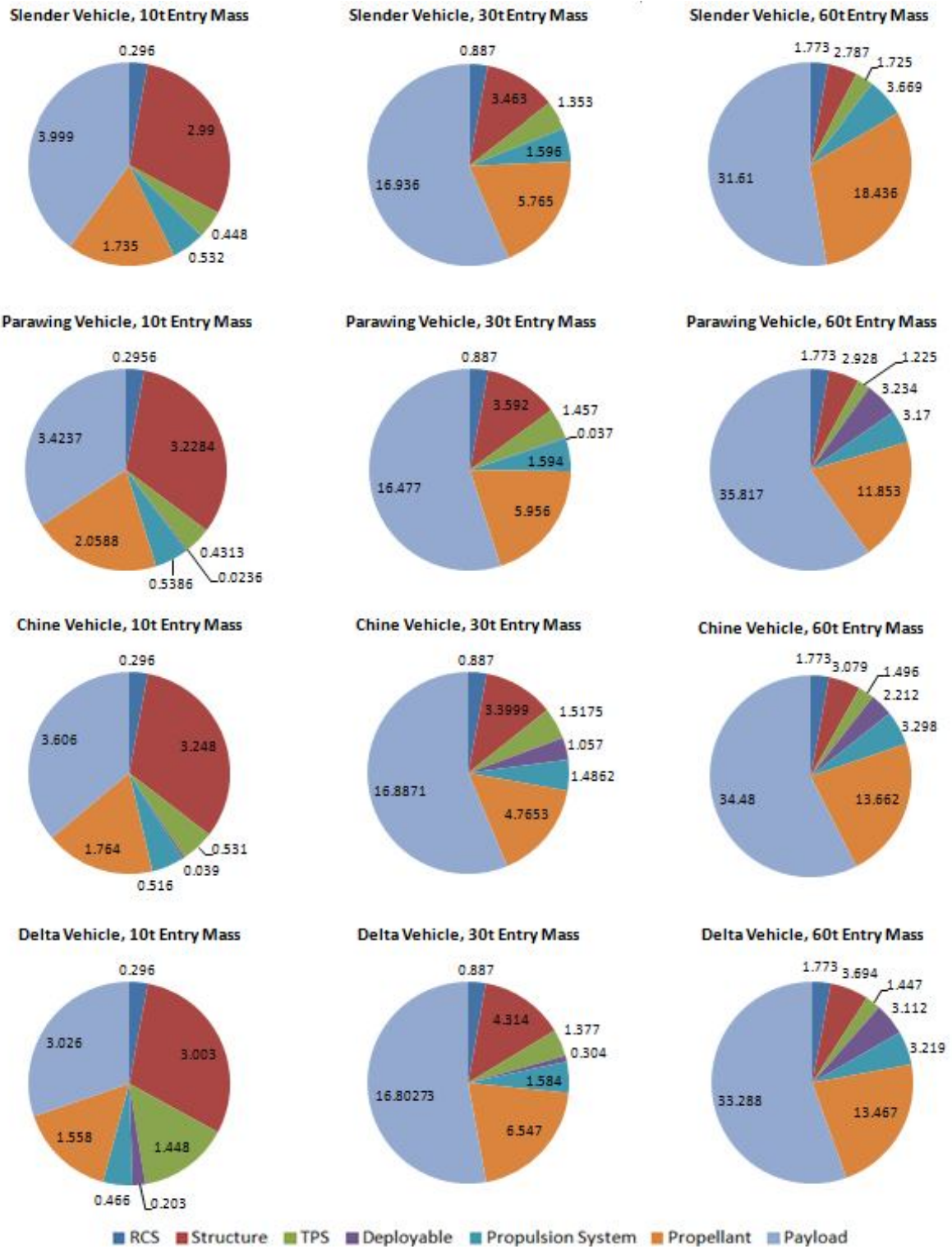


Figure 10. System mass breakdown for 10t, 30t and 60t entry mass cases.

D. Aerodynamic Heating Comparison

Figure 11 shows the maximum heat flux experienced by the vehicles on their critical heating points, normalized by the heat flux constraint value. The slender vehicle curve is the farthest from hitting the constraint due to the higher heat flux capability of the rigid TPS materials. The three deployable concepts are much closer to hitting the constraint of 150 W/cm^2 . To investigate the sensitivity of the payload mass fraction results to a lower heating constraint, the delta vehicle analysis was run using a 100 W/cm^2 constraint. The results showed that the 10t case was not affected as it did not hit the constraint, but the 20t payload mass fraction was reduced by 6%, the 30t payload mass fraction was reduced by 9%, and for the 40 to 60t cases the optimizer failed to find any feasible solutions. This demonstrates that the results are very sensitive to heating constraints, and that highly capable flexible TPS systems are required to enable these concepts.

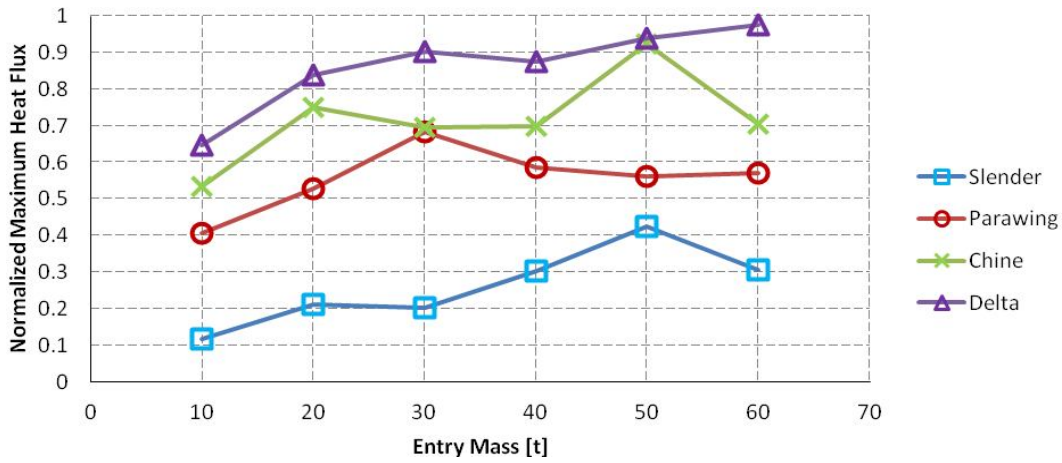


Figure 11. Maximum heat flux experienced during trajectory, normalized to heat flux constraint.

The optimized geometries for a number of selected maximum heating cases were analyzed in CBAERO to obtain estimates of the surface heat flux and temperature distributions. The dynamic pressure and Mach number conditions were selected as the highest heat flux points in the trajectory. A free-transition turbulence model was used for the chine and delta vehicles, while a laminar model was used for the parawing vehicle. These results are presented in Figure 12.

The surface temperature results for the parawing show that the temperature on the leading edges exceeds the C/SiC temperature limits by 35%. This could be reasonably fixed by adding a layer of rigid TPS material to the leading edges. The canopy heating is 85 W/cm^2 , when augmented by a factor of 5 to account for shock interaction heating. This number lies within the carbon cloth limit of 150 W/cm^2 .

The chine and delta concepts show that the maximum heating experienced by the deployables is within the 150 W/cm^2 limit. The results for the delta concept expose a design weakness, which is the heating concentration which occurs at the leading edge near the nose, due to the small radius of curvature. This causes the delta vehicle to be much closer to heating the constraint than the other two concepts. This could be alleviated through a more detailed and optimized design of the deployable geometry.

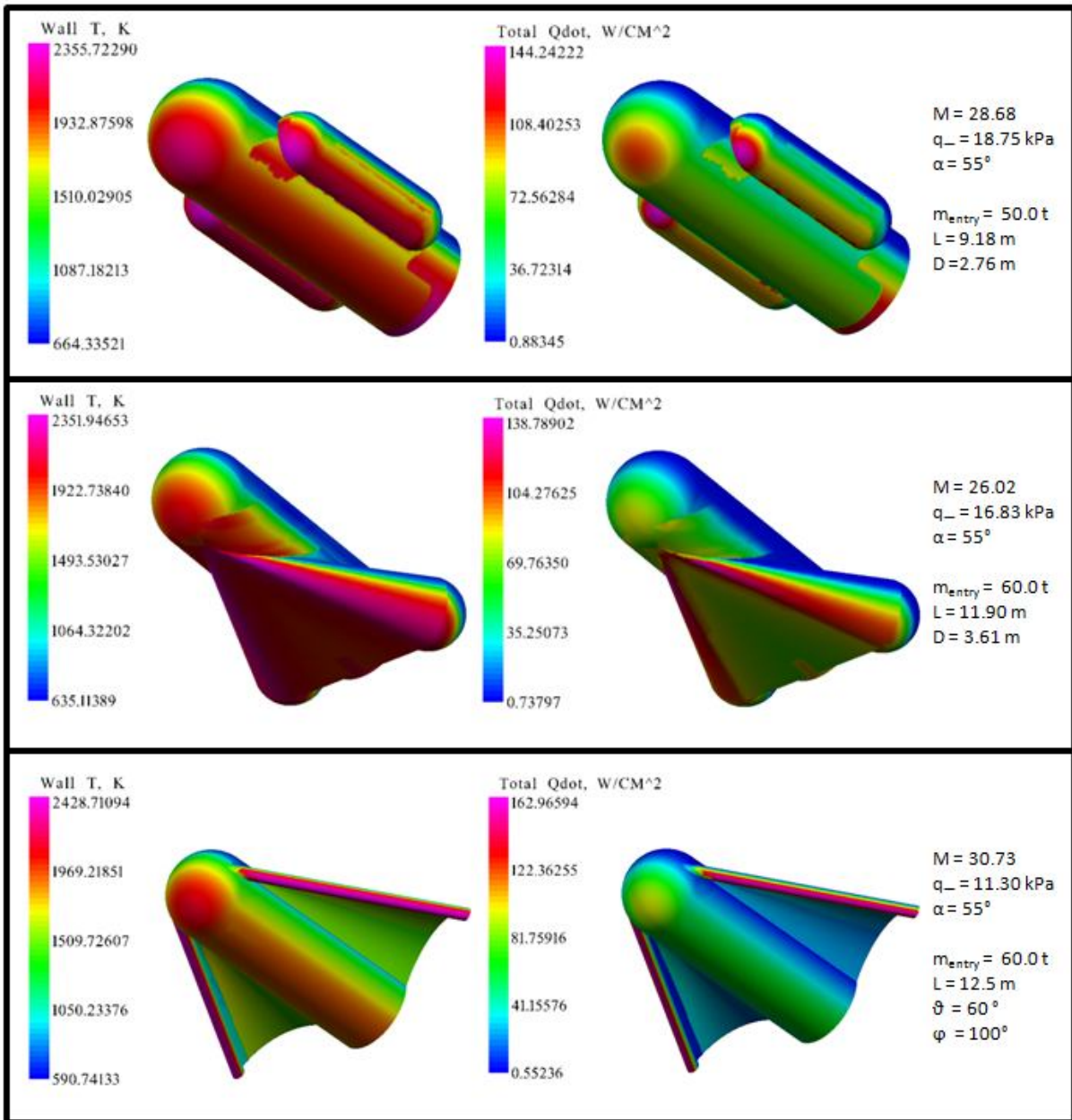


Figure 12. CBAERO aerothermodynamic heating results.

E. Trajectory Comparison

Figure 13 shows the maximum acceleration experienced by the vehicles, normalized by the constraint value of 10 Earth g's. The plot shows that the acceleration constraint is generally not the limiting factor for the performance of these systems. There is no clear distinction between the acceleration experienced by the baseline vehicle and the deployable vehicles. Figure 14 shows a plot of terminal descent initiation Mach number. At the higher entry masses, there is a clear trend showing that the deployables can reduce the terminal Mach number by about 35%. However it should be noted that all the initiation conditions are supersonic, meaning that supersonic retropropulsion is still required. These results are very sensitive to the terminal descent thrust-to-weight ratio used. If higher thrust values are allowed, the retropropulsion could be initiated later, giving the vehicle more time to slow down.

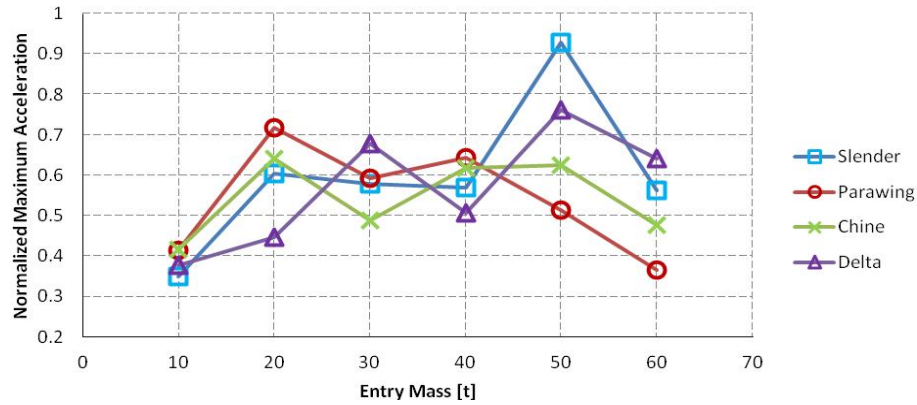


Figure 13. Maximum acceleration experienced during trajectory, normalized to acceleration constraint.

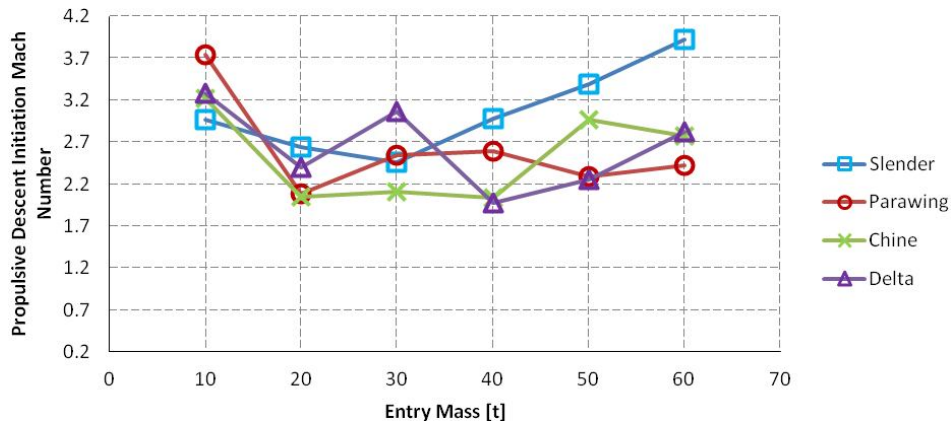


Figure 14. Mach number at propulsive descent initiation conditions.

V. Conclusion

This study presents an engineering-level exploratory study into the landed mass performance and feasibility of using deployable aerosurfaces on slender entry vehicles for a robotic-class mission at Mars. It has been shown that, based on packaging density and launch vehicle shroud constraints, a 5 meter diameter slender vehicle can enable missions with entry masses ranging from 15t to 60t, beyond what is achievable by 5 meter diameter blunt vehicles. Additionally, the performance of the slender vehicle can be improved on the 40t to 60t entry mass range by the use of a deployable system. The three deployable alternatives studied showed performance gains of up to 16% landed mass increase relative to the slender vehicle. The parawing system showed the most promise in terms of landed mass performance due to the large drag area increases achievable by this system. However, it was also limited by aerodynamic heating effects particular to this configuration, and the vehicle is not statically stable in supersonic conditions. The chine and delta deployable configurations provided simpler alternatives with lower performance. The chine concept is recommended over the delta deployable, given that it is lighter and simpler, experiences less heating, and its performance is indistinguishable from that of the delta deployable. All the deployable concepts were shown to be potentially feasible in terms of hypersonic static stability, mechanical and thermal material capabilities. However, these concepts would require flexible TPS systems capable of withstanding a momentary peak heat flux of 150 W/cm^2 , a number which stretches current flexible TPS capabilities.

Future work could focus on exploring potential capabilities of slender body deployable systems. For the parawing system, the use of inflatable leading edges and continuous wing sweep modulation during entry should be considered. The impact of the deployables on other performance parameters such as landing ellipse size and landing site elevation can also be studied. Additionally, the combination of these systems with a more capable supersonic deceleration system can be investigated. These systems could also be explored for a 10-meter diameter vehicle, which could be launched by future heavy-launchers such as the SLS. It is also recommended that more detailed feasibility studies be carried out on these concepts including dynamic stability studies, fluid-structure interaction studies, and higher fidelity aero-thermodynamic analyses.

Acknowledgments

The author would like to acknowledge the assistance of Molly Bittner in the development of the deployable mass models.

References

- [1] Braun, Robert D., and Robert M. Manning. "Mars exploration entry, descent and landing challenges." *Aerospace Conference, 2006 IEEE*. IEEE.
- [2] Garcia J. A., Brown J. L., Kinney D. J., Melton J. E., Bowles J. V., and Huynh L. C., "Co-optimized Aero Parafoil Entry (CAPE) Concepts", NASA TM-2013-XXXX, Nov, 2013
- [3] DwyerCianciolo, Alicia M., et al. "Entry, Descent and Landing Systems Analysis Study: Phase 1 Report." (2010).
- [4] Korzun, Ashley Marie. "Aerodynamic and performance characterization of supersonic retropropulsion for application to planetary entry and descent.", 2012, pp. 68 – 74.
- [5] Steinfeldt, Bradley A., et al. "High Mass Mars Entry, Descent, and Landing Architecture Assessment." *AIAA Paper* 6684 (2009).
- [6] Fournier, Paul G., and B. Bell. *Low Subsonic Pressure Distributions on Three Rigid Wings Simulating Paragliders with Varied Canopy Curvature and Leading-Edge Sweep*. No. TN D 983. NATIONAL AERONAUTICS AND SPACE ADMINISTRATION WASHINGTON DC, 1961.
- [7] Bell, B. A., and P. G. Fournier. "TRANSONIC PRESSURE DISTRIBUTIONS ON THREE RIGID WINGS SIMULATING PARAGLIDERS WITH VARIED CANOPY CURVATURE AND LEADING-EDGE SWEEP." (1962).
- [8] Fournier, Paul G. "Pressure Distributions on Three Rigid Wings Simulating Parawings with Varied Canopy Curvature and Leading-edge Sweep at Mach Numbers from 2.29 to 4.65." (1963).
- [9] Keville, Jesse F. *Semi-Rigid or Non-Rigid Structures for Re-Entry Applications. Part 1. Evaluation and Design*. No. SG-335-47-PT-1. SPACE-GENERAL EL MONTE CA, 1967.
- [10] Cruz-Ayoroa J. G., Garcia J. A., and Melton, J. E., "Validation of CFD Simulations for Parawing Geometries in Subsonic and Supersonic Flows", NASA TM-2013-XXXX, Nov. 2013.
- [11] Miihlatzter, A., and H. Pfeiffer. "CMC body flaps for the X-38 experimental space vehicle." *26th Annual Conference on Composites, Advanced Ceramics, Materials, and Structures-A: Ceramic Engineering and Science Proceedings*. Vol. 258. Wiley-American Ceramic Society, 2009.
- [12] Venkatapathy, Ethiraj, et al. "Adaptive Deployable Entry and Placement Technology (ADEPT): A Feasibility Study for Human Missions to Mars." *21st AIAA Aerodynamic Decelerator Systems Technology Conference and Seminar, Dublin, Ireland, AIAA Paper*. No. 2011-2608. 2011.
- [13] DelCorso, Joseph A., et al. "Advanced High-Temperature Flexible TPS for Inflatable Aerodynamic Decelerators." (2011).
- [14] Grant, Michael J., and G. F. Mendeck. "Mars science laboratory entry optimization using particle swarm methodology." *Proceedings of AIAA Atmospheric Flight Mechanics Conference and Exhibit, Hilton Head, South Carolina*. 2007.
- [15] Fralich, Robert. *Stress and shape analysis of a paraglider wing*. Diss. Virginia Polytechnic Institute, 1963.
- [16] Kinney, David J. "Approximate Entropy Layer Swallowing Model for the Engineering Level Aerothermodynamics Code CBAERO."
- [17] N.X. Vinh, A. Busemann, and R.D. Culp, *Hypersonic and Planetary Entry Flight Mechanics*, University of Michigan Press: Ann Arbor, Michigan, 1980.
- [18] Samareh, Jamshid A., and D. R. Komar. "Parametric Mass Modeling for Mars Entry, Descent and Landing System Analysis Study." (2011).
- [19] Cowart, Karl K., and John R. Olds. "TCAT-A tool for automated thermal protection system design." (2000).
- [20] Clark, Ian Gauld. "Aerodynamic design, analysis, and validation of a supersonic inflatable decelerator." (2009), p. 38.
- [21] Christian, John A., et al. "Extension of traditional entry, descent, and landing technologies for human Mars exploration." *Journal of Spacecraft and Rockets* 45.1 (2008): 130-141.
- [22] Korzun, A.; Braun, R.D.; "Supersonic Retropropulsion Technology for Application to High Mass Mars Entry, Descent, and Landing," May 2008.
- [23] Olstad, Walter B. "A study of the Feasibility of Inflatable Reentry Gliders." NASA, October 1960.
- [24] Powell, R. W., et al. "Performance Assessment of Aero-Assisted Orbital Transfer Vehicles," NASA, April 1984.